We are IntechOpen, the world's leading publisher of Open Access books Built by scientists, for scientists

4,800
Open access books available

122,000
International authors and editors

135M
Downloads

Our authors are among the

154
Countries delivered to

TOP 1%
most cited scientists

12.2%
Contributors from top 500 universities

CLARIVATE ANALYTICS BOOK CITATION INDEX INDEXED

WEB OF SCIENCE™

Selection of our books indexed in the Book Citation Index in Web of Science™ Core Collection (BKCI)

Interested in publishing with us?
Contact book.department@intechopen.com

Numbers displayed above are based on latest data collected.
For more information visit www.intechopen.com

Chapter 1

Hydroforming Process: Identification of the Material's Characteristics and Reliability Analysis

A. El Hami, B. Radi and A. Cherouat

Additional information is available at the end of the chapter

http://dx.doi.org/10.5772/48074

1. Introduction

The increasing application of hydroforming techniques in automotive and aerospace industries is due to its advantages over classical processes as stamping or welding. Particularly, tube hydroforming with various cross sectional shapes along the tube axis is a well-known and wide used technology for mass production, due to the improvement in computer controls and high pressure hydraulic systems (Asnafi et al., 2000; Hama et al, 2006; Cherouat et al., 2002). Many experimental studies of asymmetric hydroforming tube have been examined (Donald et al., 2000; Sokolowski et al., 2000). Theoretical models have been constructed to show the hydroforming limits, the material and the process parameters influence on the formability of the tube without failure (buckling and fracture) (Sokolowski et al.,2000). Due to the complexity of the process, theoretical studies up to date have produced relatively limited results corresponding the failure prediction. As for many other metal or sheet forming processes, the tendency of getting a more and more geometric complicated part demands a systematic numerical simulation of the hydroforming processes. This allows modifying virtually the process conditions in order to find the best process parameters for the final product. Thus, it gives an efficient way to reduce cost and time.

Many studies have been devoted to the mechanical and numerical modelling of the hydroforming processes using the finite element analysis (Hama et al., 2006; Donald et al., 2000), allowing the prediction of the material flow and the contact boundary evolution during the process. However, the main difficulty in many hydroforming processes is to find the convenient control of the evolution of the applied internal pressure and axial forces paths. This avoids the plastic flow localization leading to buckling or fracture of the tube during the process. In fact, when a metallic material is formed by such processes, it

experiences large plastic deformations, leading to the formation of high strain localization zones and, consequently, to the onset of micro-defects or cracks. This damage initiation and its evolution cause the loss of the formed piece and indicate that the forming process itself should be modified to avoid the damage appearance (Cherouat et al.,2002). In principle, all materials and alloys used for deep drawing or stamping can be used for hydroforming applications as well (Koç et al,2002).

This chapter presents firstly a computational approach, based on a numerical and experimental methodology to adequately study and simulate the hydroforming formability of welded tube and sheet. The experimental study is dedicated to the identification of material parameters using an optimization algorithm known as the Nelder-Mead simplex (Radi et al.,2010) from the global measure of displacement and pressure expansion. Secondly, the reliability analysis of the hydroforming process of WT is presented and the numerical results are given to validate the adopted approach and to show the importance of this analysis.

2. Hydroforming process

For production of low-weight, high-energy absorbent, and cost-effective structural automotive components, hydroforming is now considered the only method in many cases.

The principle of tube hydroforming is shown in Figure 1. The hydroforming operation is either force-controlled (the axial forces vary with the internal pressure) or stroke-controlled (the strokes vary with the internal pressure). Note that the axial force and the stroke are strongly interrelated (see figure 1).

Force-controlled hydroforming is at the focus in (Asnafi et al.,2000), where the constructed analytical models are used to show

- which are the limits during hydroforming,
- how different material and process parameters influence the loading path and the forming result, and
- what an experimental investigation into hydroforming should focus on.

The hydroforming operation comprises two stages: free forming and calibration. The portion of the deformation in which the tube expands without tool contact, is called free forming. As soon as tool contact is established, the calibration starts.

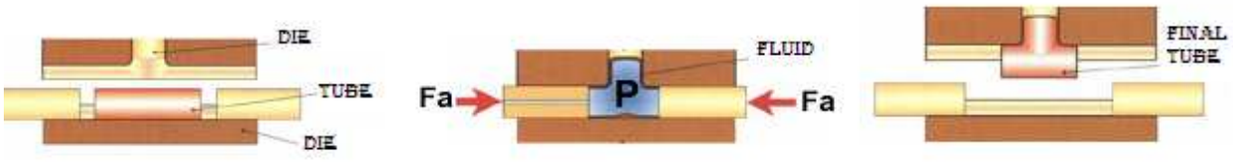

Figure 1. The principle of tube hydroforming: (a) original tube shape and (b) final tube shape (before unloading).

During calibration, no additional material is fed into the expansion zone by the axis cylinders. The tube is forced to adopt the tool shape of the increasing internal pressure only.

Many studies have been devoted to the mechanical and numerical modeling of the hydroforming processes using the finite element analysis, allowing the prediction of the material flow and the contact boundary evolution during the process. However, the main difficulty in many hydroforming processes is to find the convenient control of the evolution of the applied internal pressure and axial forces paths. This avoids the plastic flow localization leading to buckling or fracture of the tube during the process. In fact, when a metallic material is formed by such processes, it experiences large plastic deformations, leading to the formation of high strain localization zones and, consequently, to the onset of micro-defects or cracks. This damage initiation and its evolution cause the loss of the formed piece and indicate that the forming process itself should be modified to avoid the damage appearance. In principle, all materials and alloys used for deep drawing or stamping can be used for hydroforming applications as well.

2.1. Mechanical characteristic of welded tube behaviour

Taking into account the ratio thickness/diameter of the tube, the radial stress is considerably small compared to the circumferential σ_θ and longitudinal stresses σ_z (see Figure 2). In addition, the principal axes of the stress tensor and the orthotropic axes are considered coaxial. The transverse anisotropy assumption represented through the yield criterion can be written as:

$$\bar{\sigma}^2 = F\left(\sigma_z - \sigma_\theta\right)^2 + G\sigma_z^2 + H\sigma_\theta^2 \tag{1}$$

with (F,G,H) are the parameters characterizing the current state of anisotropy.

If the circumferential direction is taken as a material reference, the anisotropy effect can be characterized by a single coefficient R and the equation (1) becomes:

$$\bar{\sigma}^2 = \frac{1}{1+R}\left[R\left(\sigma_z - \sigma_\theta\right)^2 + \sigma_z^2 + \sigma_\theta^2\right] \tag{2}$$

The assumptions of normality and consistency lead to the following equations:

$$\begin{cases} d\varepsilon_\theta = \dfrac{d\bar{\varepsilon}}{\bar{\sigma}}\left(\sigma_\theta - \dfrac{R}{1+R}\sigma_z\right) \\ d\varepsilon_z = \dfrac{d\bar{\varepsilon}}{\bar{\sigma}}\left(\sigma_z - \dfrac{R}{1+R}\sigma_\theta\right) \end{cases} \tag{3}$$

where $\bar{\varepsilon}$ is the effective plastic strain and $\left(\varepsilon_\theta, \varepsilon_z\right)$ are the strains in the circumferential and the axial directions. The effective strain for anisotropic material can be derived from equivalent plastic work definition, incompressibility condition, and the normality condition:

$$d\bar{\varepsilon} = \frac{\sqrt{1+R}}{\sqrt{1+2R}}\sqrt{d\varepsilon_z^2 + d\varepsilon_\theta^2 + R\left(d\varepsilon_z - d\varepsilon_\theta\right)^2} = \left(\sqrt{\gamma^2 + \frac{2R}{1+R}\gamma + 1}\right)\frac{1+R}{\sqrt{1+2R}}d\varepsilon_\theta \quad \text{with} \quad \gamma = \frac{d\varepsilon_z}{d\varepsilon_\theta} \tag{4}$$

Taking into account the relations expressing strain tensor increments, the equivalent stress (Equation 2) becomes:

$$\bar{\sigma} = \left(\sqrt{1 + \gamma^2 + \frac{2R}{1+R}\gamma} \right) \frac{\sqrt{1+2R}}{1+R+R\gamma} \sigma_\theta \tag{5}$$

In the studied case, the tube ends are fixed. As a consequence, the longitudinal increment strain $d\varepsilon_z = 0$, and then relations (4) and (5) become:

$$\bar{\sigma} = \left(\sqrt{\frac{2R^2 + 3R + 1}{(1+R)^3}} \right) \sigma_\theta \qquad d\bar{\varepsilon} = \left(\frac{1+R}{\sqrt{1+2R}} \right) d\varepsilon_\theta \tag{6}$$

The knowledge of the two unknown strain ε_θ and stress σ_θ needs the establishment of the final geometric data linked to the tube (diameter and wall thickness):

$$\varepsilon_\theta = \ln\left(\frac{d}{d_0} \right) \text{ and } \sigma_\theta = \frac{Pd}{2t} \tag{7}$$

where P is the internal pressure, (d, d_0) are the respective average values of the current and initial diameter of the sample and (t) is the current wall thickness obtained according to the following relation:

$$t = t_0 e^{-(1+\gamma)\varepsilon_\theta} \tag{8}$$

Finally, the material characteristics of the tube (base metal) are expressed by the effective stress and effective strain according to the following equation (Swift model):

$$\bar{\sigma} = K(\varepsilon_0 + \bar{\varepsilon})^n \tag{9}$$

The values of the strength coefficient *K*, the strain hardening exponent *n*, the initial strain ε_0 and the anisotropic coefficient R in Equations (2) and (9) are identified numerically. For the determination of the stress–strain relationship using bulge test, the radial displacement, the internal pressure and the thickness at the center of the tube are required.

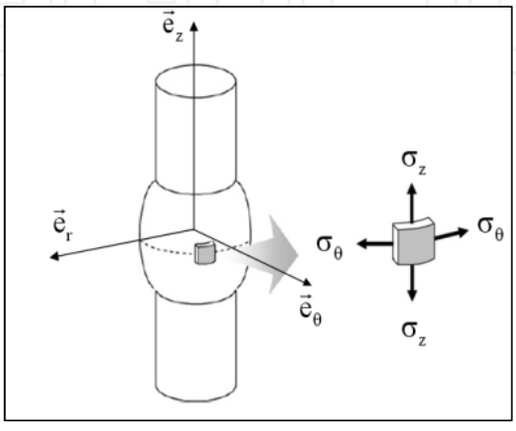

Figure 2. Stress state at bulge tip

3. Identification process

The parameters (K, ε_0, n) are computed in such a way that the constitutive equations associated to the yield surface reproduce as well as possible the following characteristics of the sheet metal. The problem which remains to be solved consists in finding the best combination of the parameters damage which minimizes the difference between numerical forecasts and experimental results. This minimization related to the differences between the m experimental measurements of the tensions and their numerical forecasts conducted on tensile specimens.

Due to the complexity of the used formulas, we have developed a numerical minimization strategy based on the Nelder-Mead simplex method. The identification technique of the material parameters is based on the coupling between the Nelder-Mead simplex method (Matlab code) and the numerical simulation based finite element method via ABAQUS/Explicit© of the hydroforming process. To obtain information from the output file of the ABAQUS/Explicit©, we use a developed Python code (see Figure 3).

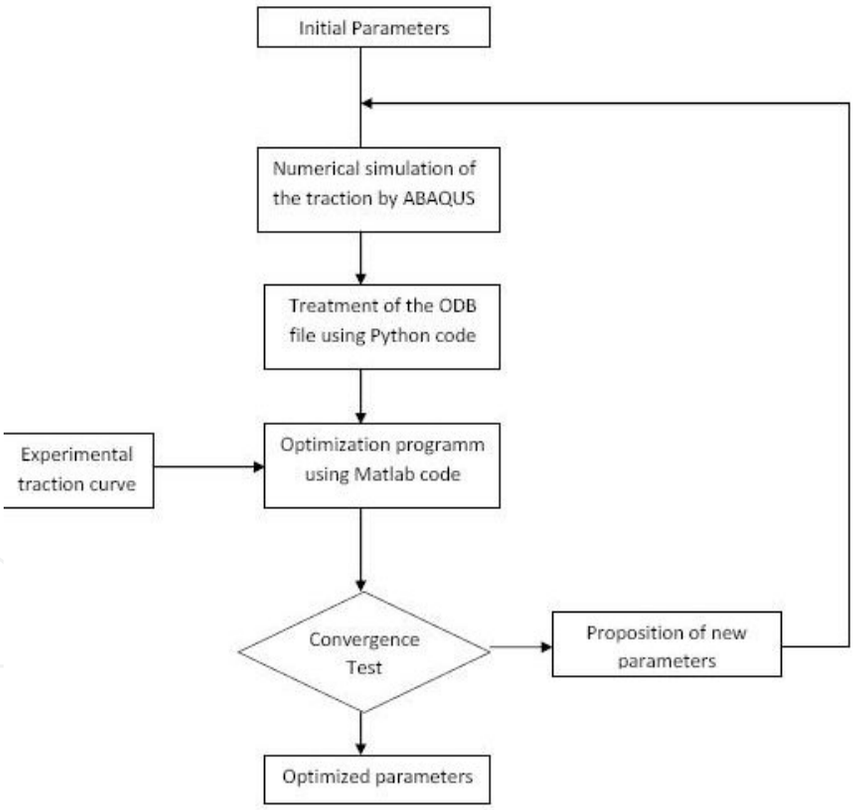

Figure 3. Identification process

4. Results and discussion

A three dimensional finite element analysis (FEA) has been performed using the finite element code ABAQUS/Explicit to investigate the hydroforming processes.

4.1. Tensile test

Rectangular specimens are made with the following geometric characteristics: thickness=1.0mm, width=12.52mm and initial length=100mm, were cut from stainless (Figure 4). All the numerical simulations were conducted under a controlled displacement condition with the constant velocity v=0.1mm/s. The predicted force versus displacement curves compared to the experimental results for the three studied orientations are shown in Figure 1. With small ductility (Step 1) the maximum stress is about 360MPa reached for 25% of plastic strain and the final fracture is obtained for 45% of plastic strain. With moderate ductility (Step 3) the maximum stress is about 394MPa reached in 37.2% of plastic strain and the final fracture is obtained for 53% of plastic strain. The best values of the material parameters using optimization procedure are summarized in Table 1. Within these coefficients the response (stress versus plastic strain) presents a non linear isotropic hardening with a maximum stress $\sigma_{max} = 279$ MPa reached in $\bar{\varepsilon}^p = 36.8\%$ of plastic strain and the final fracture is obtained for 22 % of plastic strain. The plastic strain map of the optimal case is presented in Figure 1.

Step	Critical plastic strain	K [MPa]	ε_0	n
1	25,8%	381,3	0.0100	0.2400
2	29,8%	395,5	0.0120	0.2415
3	37,2%	415,2	0.0150	0.2450
Optimal	36,8%	416,1	0.0198	0.2498

Table 1. Properties of the used material

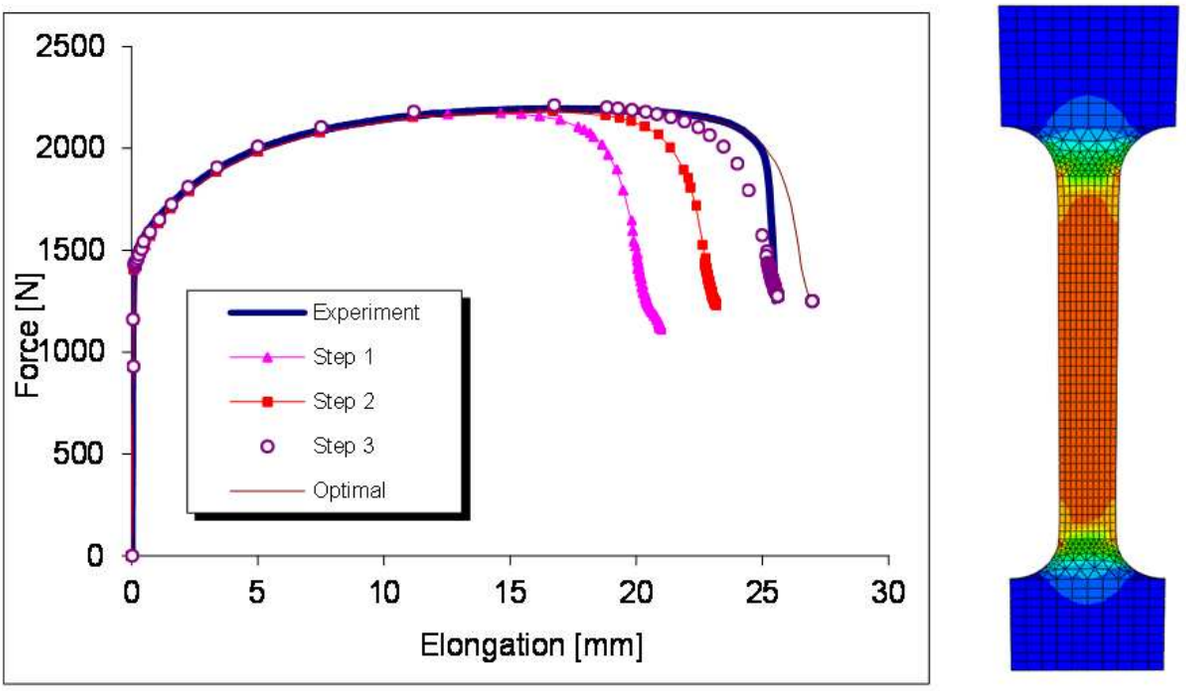

Figure 4. Force/elongation for different optimization steps and plastic strain map

4.2. Welded tube (WT) hydroforming process

In this case, the BM with geometrical singularities found in the WT is supposed orthotropic transverse, whereas its behaviour is represented by Swift model. The optical microscope observation on the cross section of the wall is used to build the geometrical profile of the notch generated by the welded junction. By considering the assumptions relating to an isotropic thin shell (R=1) with a uniform thickness, the previously established relations (6), (7) and (9) allow to build the first experimental hardening model using measurements of internal pressure/radial displacements. This model is then proposed, as initial solution, to solve the inverse problem of required hardening law that minimizes the following objective function:

$$\xi_F = \frac{1}{m_p}\sqrt{\sum_{i=1}^{m_p}\left(\frac{F_{exp}^i - F_{num}^i}{F_{exp}^i}\right)^2} \tag{10}$$

where F_{exp}^i is the experimental value of the thrust force corresponding to i^{th} nanoindentation depth H_i, F_{num}^i is the corresponding simulated thrust force and m_p is the total number of experimental points.

Different flow stress evolutions of isotropic hardening (initial, intermediate and optimal) are proposed in order to estimate the best behavior of the BM with geometrical singularities found in the WT. Figures 5 and 6 show the effective stress versus plastic strain curves and the associate pressure/radial displacement for these three cases. As it can be seen, there is a good correlation between the optimal evolution of Swift hardening and the experimental results. Table 1 summarizes the parameters of these models.

Hardening model	ε_0	K (MPa)	n
Initial	0.025	1124.6	0.2941
Intermediate	0.055	692.30	0.2101
Optimal	0.080	742.50	0.2359

Table 2. Swift parameters of different hardening evolution

The anisotropy factor R is determined only for the optimal hardening evolution. In the problem to be solved there is only one parameter which initial solution exists, that it corresponds to the case of isotropic material (R = 1). The numerical iterations were performed on the WT with non-uniformity of the thickness (see Figure 7), and the obtained results are shown in Figure 8. A good improvement in the quality of predicted results is noted if R corresponds the value of 0.976.

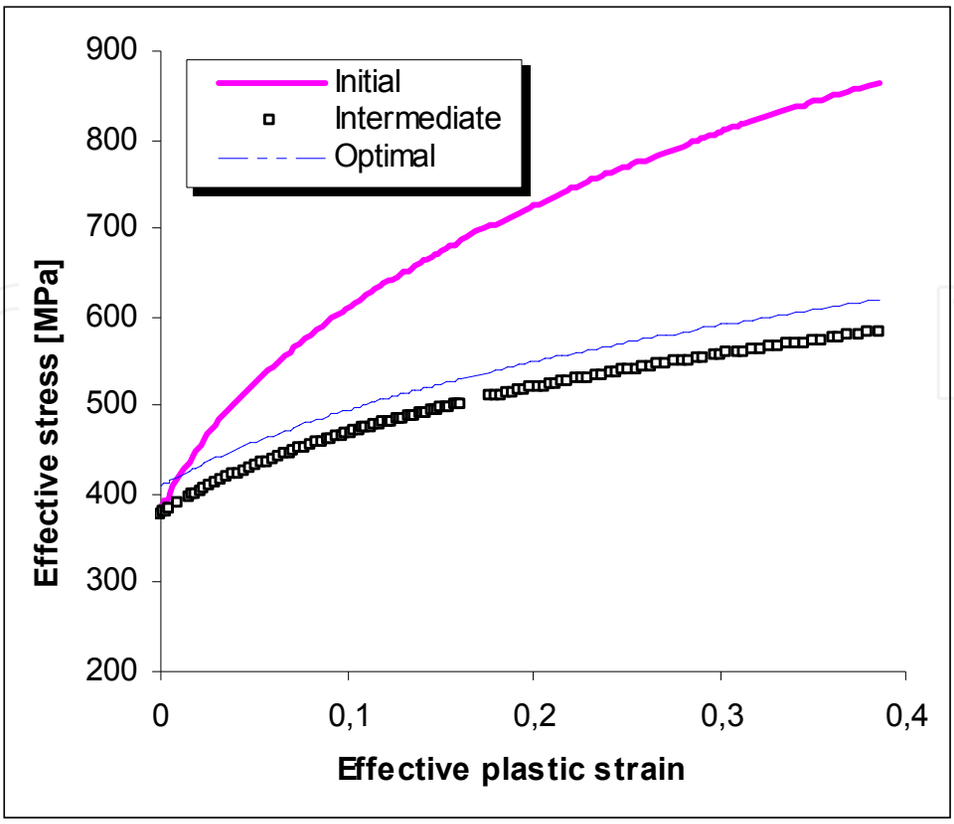

Figure 5. Stress-strain evolutions for different hardening laws

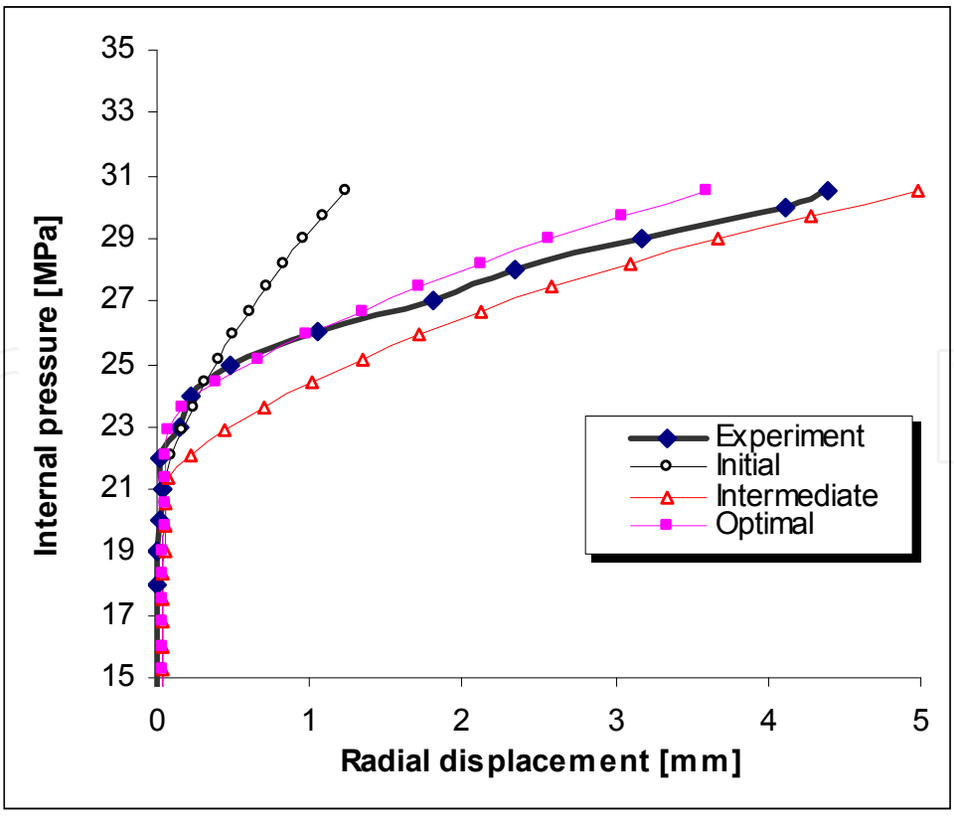

Figure 6. Internal pressure versus radial displacement

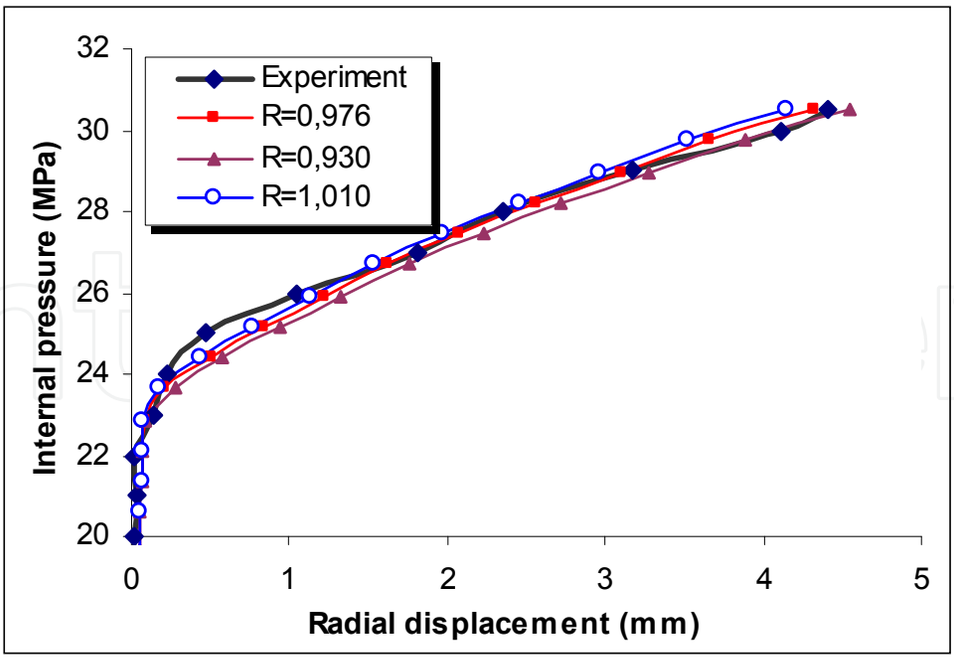

Figure 7. Radial displacement for different values of anisotropy coefficient R

4.3. Thin sheet hydroforming process

Sheet metal forming examples will be presented in order to test the capability of the proposed methodology to simulate thin sheet hydroforming operation using the fully isotropic model concerning elasticity and plasticity (Cherouat et al.,2008). These results are carried out on the circular part with a diameter of 300mm and thickness of 0.6mm. During hydroforming of the blank sheet, the die shape keeps touching the blank, which prevents the deformed area from further deformation and makes the deformation area move towards the outside. The blank flange is drawn into the female die, which abates thinning deformation of deformed area and aids the deformation of touching the female die and uniformity of deformation. Compared with the experiments done before, the limit drawing ratio of the blank is improved remarkably.

By considering the assumptions relating to an isotropic thin shell with a uniform thickness, the previously established relations allow to build the first experimental hardening model using measurements of force/displacement. This model is then proposed, as initial solution, to solve the inverse problem of required hardening law that minimizes the following objective function:

$$E_{error} = \frac{1}{m}\sqrt{\sum_{1}^{m}\left(\frac{P_{exp}^{i} - P_{num}^{i}}{P_{exp}^{i}}\right)^{2}} \tag{11}$$

where P_{exp}^{i} is the experimental value of the thrust pressure corresponding to i^{th} displacement δ_i, P_{num}^{i} is the corresponding predicted pressure and m is the total number of experimental points.

The controlled process parameters are the internal fluid pressure applied to the sheet as a uniformly distributed load to the sheet inner surface and is introduced as a linearly increasing function of time with a constant flow from approximately 10 ml/min. The comparator is used to measure the pole displacement. The effect of three die cavities (D1, D2 and D3 see Figure 8) on the plastic flow and damage localisation is investigated during sheet hydroforming. These dies cavities are made of a succession of revolution surfaces (conical, planes, spherical concave and convex). The evolution of displacement to the poles according to the internal pressure during the forming test and sheet thicknesses are investigated experimentally. The profiles of displacements are obtained starting from the deformations of the sheet after bursting. Those are reconstituted using 3D scanner type Dr. Picza Roland of an accuracy of 5μm with a step of regulated touch to 5mm. In addition, two measurement techniques were used to evaluate the thinning of sheet after forming; namely a non-destructive technique using an ultrasonic source of Sofranel mark (Model 26MG) and a destructive technique using a digital micrometer calliper of Mitiyuta mark of precision 10μm (see Figure 9).

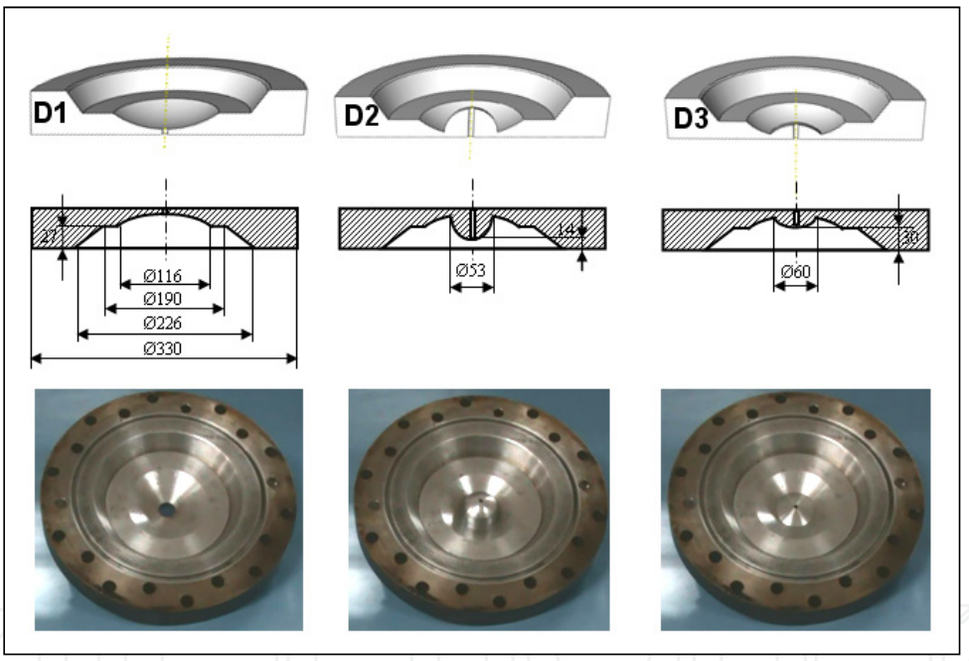

Figure 8. Geometry of die cavities (D1, D2 and D3)

Experiments results of circular sheet hydroforming are shown in Figure 10 (Die D1), Figure 11 (Die D2) and Figure 12 (Die D3). For the die cavities D1 and D3, fracture appeared at the round corner (near the border areas between the conical and the hemispherical surfaces of the die). For the die cavity D2, the fracture occurred at the centre of the blank when the pressure is excessive. This shows that the critical deformation occurs at these regions. It is noted that the rupture zone depends on the die overflow of the pressure medium from the pressurized chamber and the reverse-bending effect on the die shoulder were not observed in the experiment. In this part we are interested in the comparison between experimental observations of regions where damage occurred and numerical predictions of areas covered

by plastic instability and damage. Figures 10, 11 and 12 present as such, the main results and simulations of all applications processed in this study. The predicted results with cavity dies show that the equivalent von Mises stress reached critical values high and then subjected to a significant decrease in damaged areas. This decrease is estimated for the three die cavities D1, D2 and D3, respectively 29%, 14% and 36%.

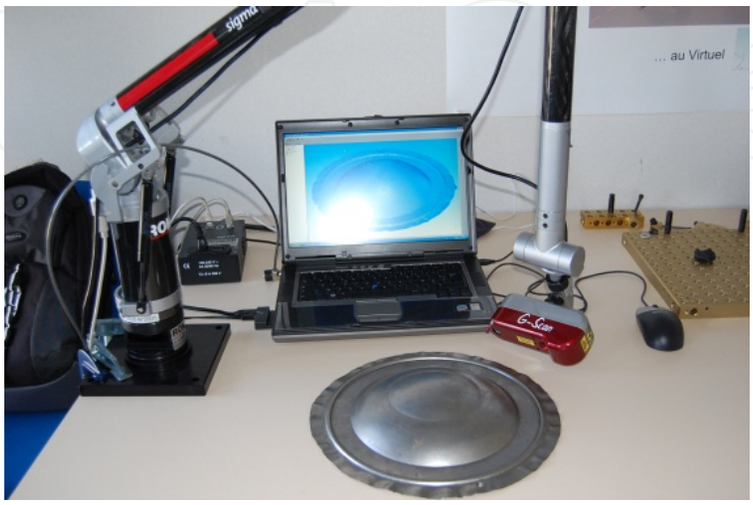

Figure 9. 3D scanner G Scan for reconstitution

Comparisons between numerical predictions of damaged areas and the experimental observations of fracture zones led us to the following findings:

1. The numerical calculations show that increasing pressure, the growing regions marked by a rise in the equivalent stress followed by a sudden decrease can be correlated with the damaged zones observed experimentally. In this context, the results of the first die cavity D1 show that instabilities are localized in the central zone of the blank, limited by a circular contour of the radius 72mm. The largest decrease in stress is located in the area bounded by two edges of respective radii 51 and 64mm. While the rupture occurred at the border on the flat surface with the spherical one located on a circle of radius 60mm. With the die cavity D2, the largest decrease is between two contours of radii 10 and 19mm, the rupture is observed at a distance of 17mm from the revolution axis of deformed blank. Finally with the die cavity D3, the calculations show that the damaged area is located in a region bounded by two edges of respective radii 54 and 73mm, the rupture occurred in the connection of the flat surface with the surface spherical one.
2. The pressures that characterize the early instabilities are respectively the order of 4.90MPa (for D1), 2.85MPa (for D2) and 5.1MPa (for D3). For applications with die cavities D1 and D3, regions where the beginnings of instability have been identified (see Table 2).

The results presented in Fig. 9 show that the relative differences between predicted and experiment results of pole displacement are in the limit of 7% while the pressure levels are below a threshold characterizing the type of application.

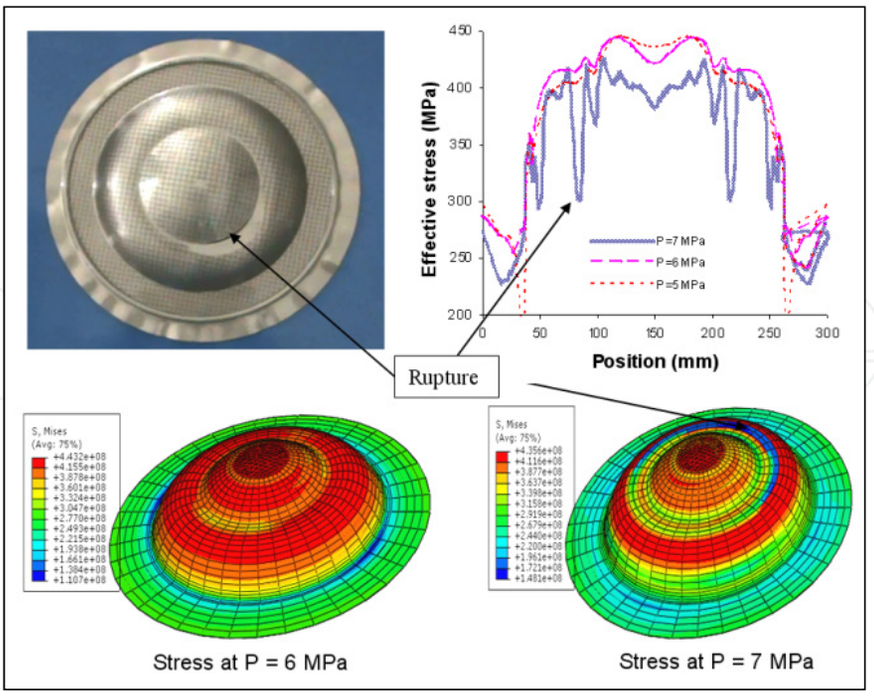

Figure 10. Experimental and numerical results of hydroforming using die cavity D1

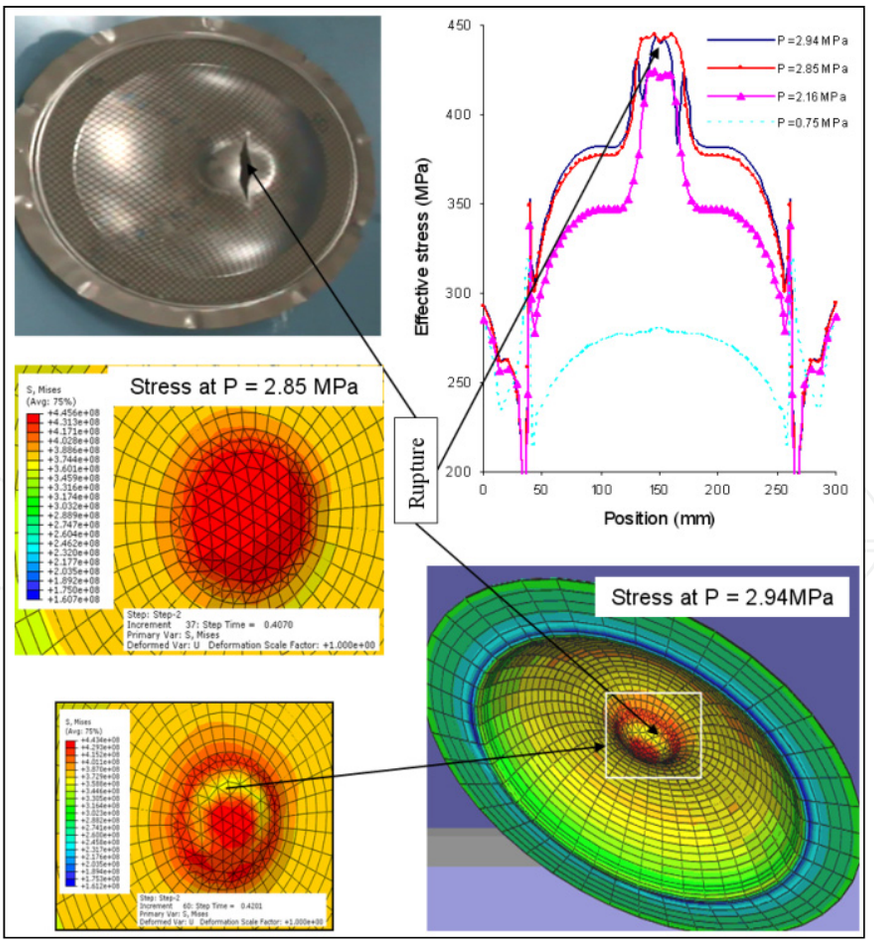

Figure 11. Experimental and numerical results of hydroforming using die cavity D2

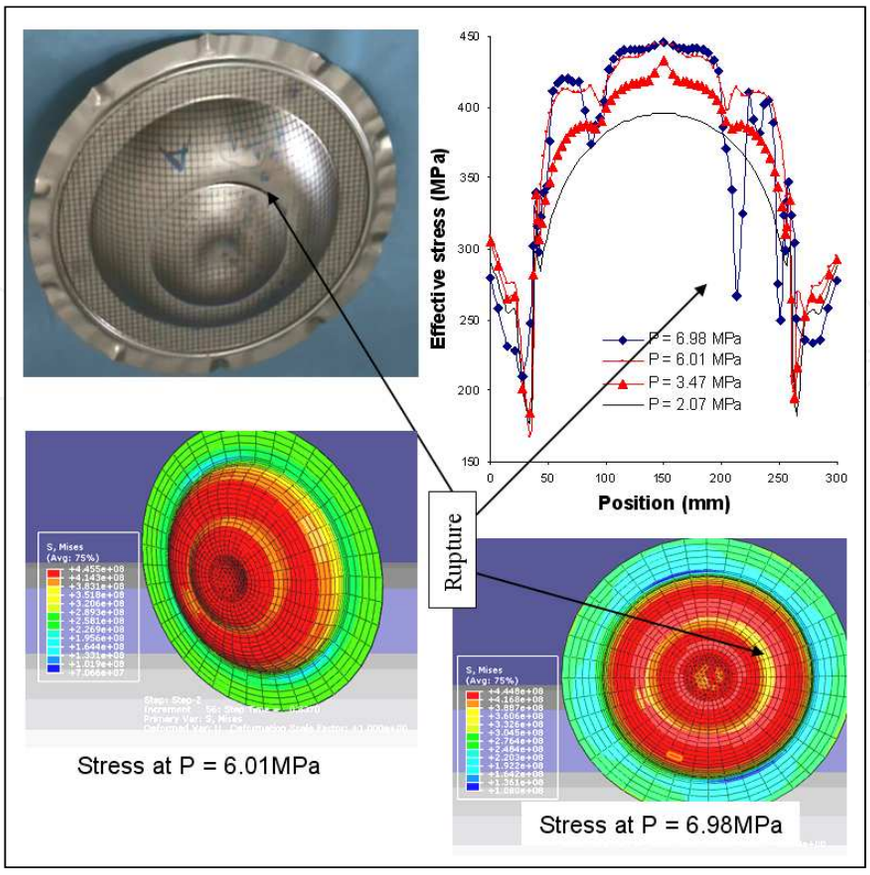

Figure 12. Experimental and numerical results of hydroforming using die cavity D3

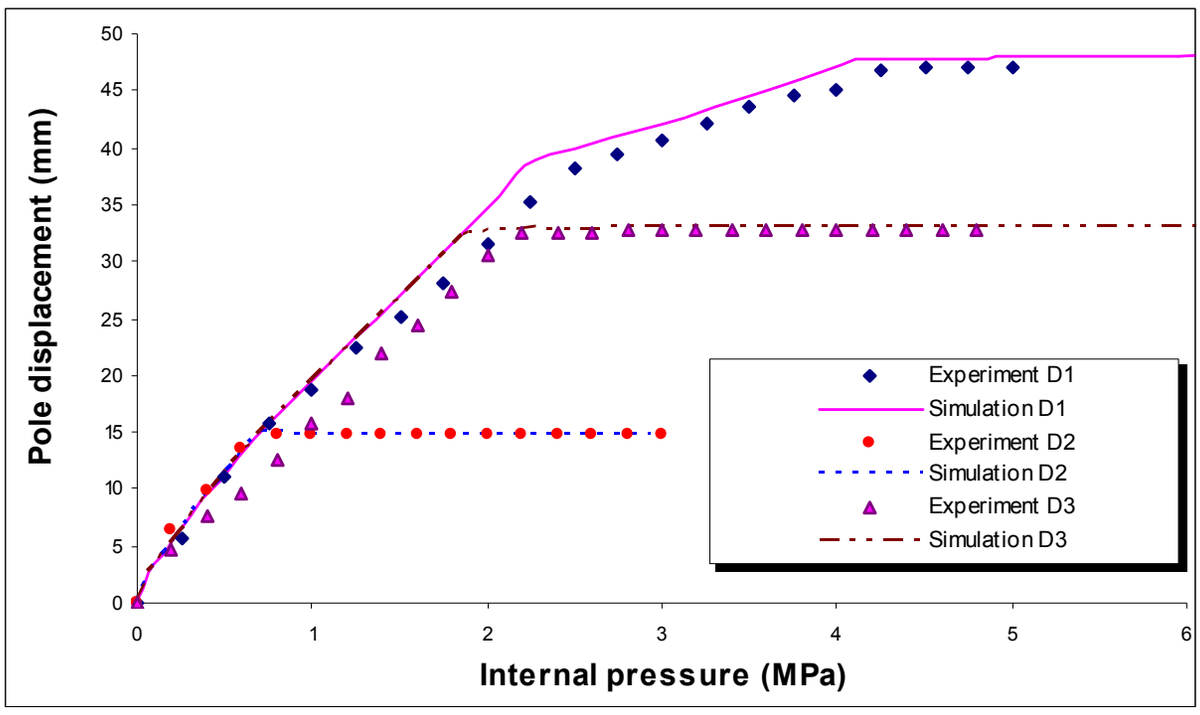

Figure 13. Pole displacement versus internal pressure

Die cavity	Beginning instability (MPa)	Critical (MPa)	Experimental (MPa)
D1	4,90	6,74	5,2
D2	2,85	2,85	3,0
D3	5,10	6,86	5,3

Table 3. Levels of pressure for different dies

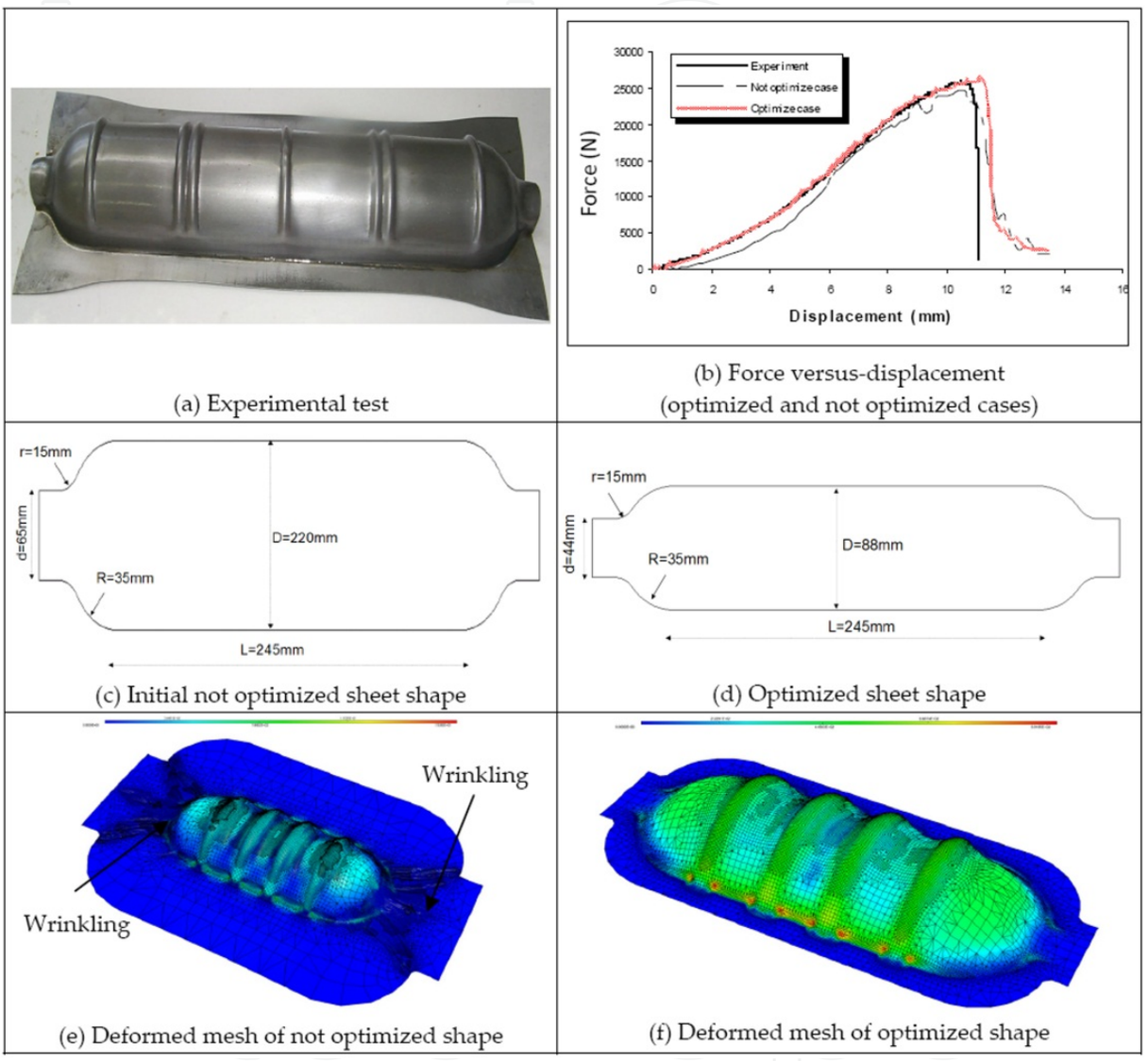

Figure 14. Optimisation of complex shape part

4.4. Optimization of sheet shape

Optimization is the action of obtaining the preferable results during the part design. In the CAE-based application of optimization, several situations can cause the numerical noise (wrinkling). When the numerical noise exists in the design analysis loop, it will create many artificial local minimums. In this case, the minimization of local thinning condition in the blank sheet metal was tested with a cost function of the optimization system was chosen to minimize the thinning ratio of 20% thinnest element.

i.e. Cost function: $f = \sum_{i=1}^{n} \left\| \frac{t - t_0}{t_0} \right\|^2$

where t_0 is the initial thickness and t the final thickness.

In this case a significant design variable for formability of blank during hydroforming process and the design (D and d) constraints were defined:

$50 \le D \le 250\text{mm}$ $20 \le d \le 100\text{mm}$. The experimental final shape is shown in Figure 10a. The comparison of the force versus the maximum displacement with the initial and optimized blank shape is present in Figure 10b. Good agreement between the optimum shape and the experimental values. Figures 10c and 10d compare the initial and the optimum blank shape. Successfully decreased the cost function (thinning ratio) from 50% to 20% is obtained without wrinkling (Figure 10e and 10f) (see Ayadi et al.,2011).

5. Reliability analysis

Recently, RBDO has become a popular philosophy to solve different kind of problem. In this part, we try to prove the ability of this strategy to optimize loading path in the case of THP where different kind of nonlinearities exist (material, geometries and boundary conditions). The aim of this study is to obtain a free defects part with a good thickness distribution, decrease the risk of potential failures and to let the process insensitive to the input parameters variations. For more detailed description of the RBDO methodology and variety of frameworks the reader can be refer to the following references (Youn et al., 2003; Enevoldsen et al., 1994; El Hami et al., 2011). The RBDO problem can be generally formulated as:

$$\begin{cases} \text{Min } f(d,X) \\ \text{subject to } P\left[G_i(d,X) \le 0\right] - \Phi\left(-\beta_{t_i}\right) \le 0 \quad i = 1,\ldots,np \\ d^L \le d \le d^U,\ d \in R^{ndv} \text{ and } X \in R^{nrv} \end{cases} \tag{12}$$

where f(d,X) is the objective function, d is the design vector, X is the random vector, and the probabilistic constraints is described by the performance function $G_i(X)$, np, ndv and nrv are the number of probabilistic constraints, design variables and random variables, respectively, β_{ti} is the prescribed confidence level which can be defined as $\beta_{t_i} = -\Phi^{-1}(P_f)$ where P_f is the probability of failure and Φ is the cumulative distribution function for standard normal distribution.

The process failure state is characterized by a limit state function or performance function G(X), and G(X)=0 denotes the limit state surface. The m-dimensional uncertainty space in thus divided into a safe region $\left(\Omega_s = \{X : G(X) > 0\}\right)$ and a failure region $\left(\Omega_f = \{X : G(X) \le 0\}\right)$ (see Radi et al.,2007).

5.1. Definition of the limit state functions

The risk of failure is estimated based on the identification of the most critical element for necking and severe thinning. For this reason fine mesh was used in this study to localize the plastic instability or the failure modes in one element. Some deterministic finite element simulations show that always severe thinning is localised in element 939 in the centre of the expansion region and necking in element 1288 as shown in Figure 22.

Since the strain\stress of element 939\1288 is the critical strain\stress of the hydroformed tube, then the reliability of these two elements represented in reality the reliability of the hydroforming process.

In this work, the limit state functions take advantage from the FLSD and the FLD of the material to assess the risk or the probability of failure of necking and severe thinning. From these curves we distinguish mainly two zones: feasible region: when a tube hydroforming process can be done in secure conditions and unfeasible region when plastic instability can appear as shown in Figures 24-25. In reality, the FLSD and FLD was used in several papers (Kleiber et al, 2004; Bing et al., 2007) as failure criteria in the aim to assess the probability of failure.

The limit state function depends on the variable of the process. Mathematically, this function can be described as $Z = G\left(\{x\},\{y\}\right)$, where $\{x\}$ presents a vector of deterministic variables and $\{y\}$ is a vector of random variables.

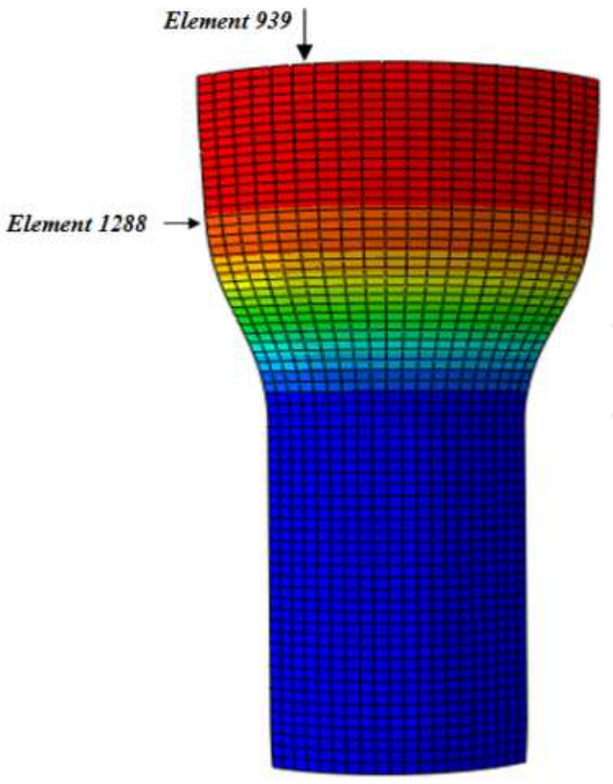

Figure 15. Location of the critical elements for severe thinning and necking

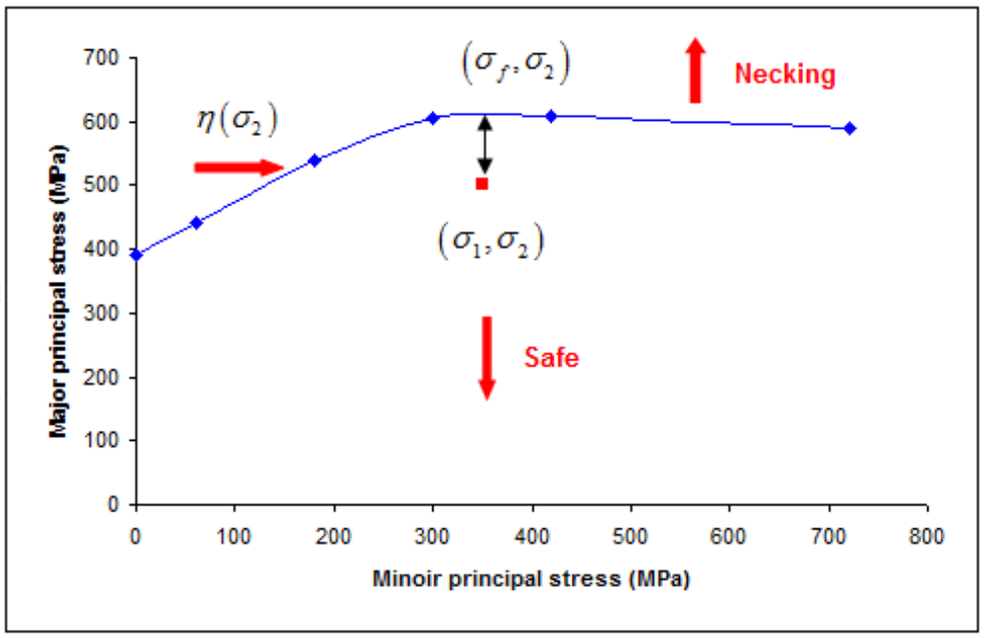

Figure 16. Forming limit stress diagram

The first limit state function was taken to be the difference between the maximum stress and the corresponding FLSD as shown in Figure 25:

$$\begin{cases} G\left(\{x\},\{y\}\right) = \sigma_f - \sigma_1^c \\ \sigma_f = \eta(\sigma_2) \end{cases} \tag{13}$$

where σ_1^c is the maximum stress in the most critical element and σ_f the corresponding forming stress limit. The role of this constraint is to maintain the maximum stress on the critical element below σ_f. The second limit state function is used to control the severe thinning in the tube, to define this function we use the FLD plotted in the strain diagram as shown in Figure 25, it can be given by the following expression:

$$\begin{cases} G\left(\{x\},\{y\}\right) = F_{th} = \sigma_f - \sigma_1^c \\ \sigma_f = \eta(\sigma_2) \end{cases} \tag{14}$$

where ε_1 is the major strain in the critical element and ε_{th} is the thinning limit determined from the FLD curve as shown in Figure 17.

The objective function consists to reduce the wrinkling tendency, this function is inspired from the FLD and given by the following expression:

$$\begin{cases} F_w = \sum_{i=1}^{N} \left(d_w^i\right)^2 = \sum_{i=1}^{N} \left(\varepsilon_1^i - \varepsilon_w^i\right)^2 \\ \varepsilon_w = \phi(\varepsilon_2) \end{cases} \tag{15}$$

where ε_1 is the major strain in element i, and ε_w is the wrinkling limit value determined from the FLD, N is the number of elements.

The success of a THP is dependent on a number of variables such as the loading paths (internal pressure versus time and axial displacement versus time), lubrication condition, and material formability. A suitable combination between all these parameters is important to avoid part failure due to wrinkling, severe thinning or necking. Koç et al. (Koç et al.,2002) found that loading path and variation in material properties has a significant effect on the robustness of the THP and final part specifications. In this work, we define the load path as design variables to be optimized.

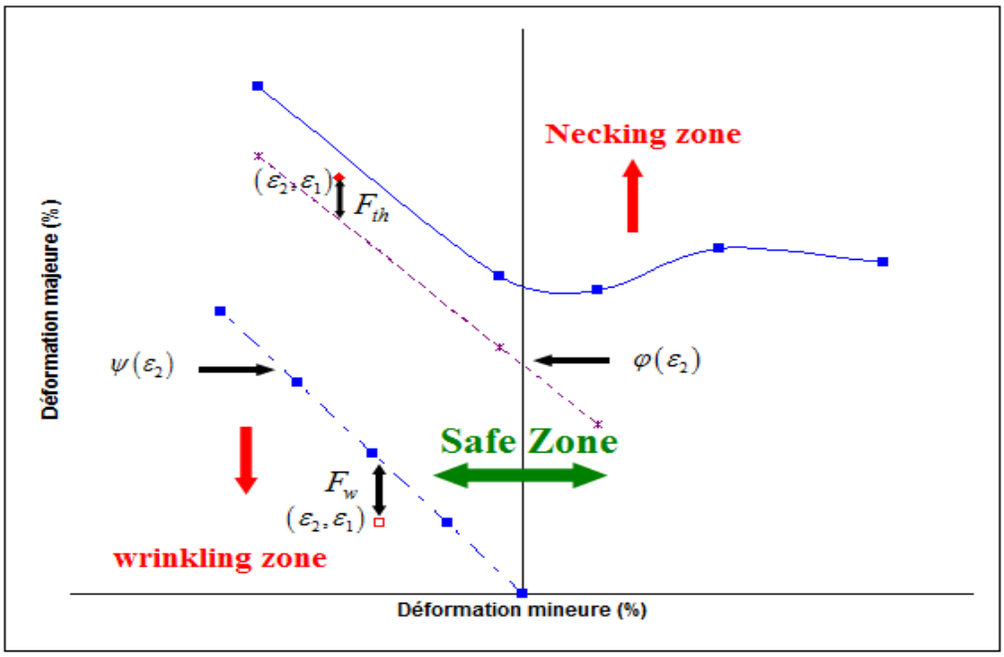

Figure 17. Forming Limit Diagram

The load path given the variation of the inner pressure vs. time is modelled by two points (P_1,P_2) displacement is imposed as a linear function of time, for axial displacement we interest only on the amplitude D. Table 4 illustrates the statistical properties of the design variables.

Variable	Mean value	Cov(%)	Distribution type
P_1 (MPa)	15	5	Normal
P_2 (MPa)	35	5	Normal
D(mm)	8	5	Normal

Table 4. Statistical properties of the control points described the load path

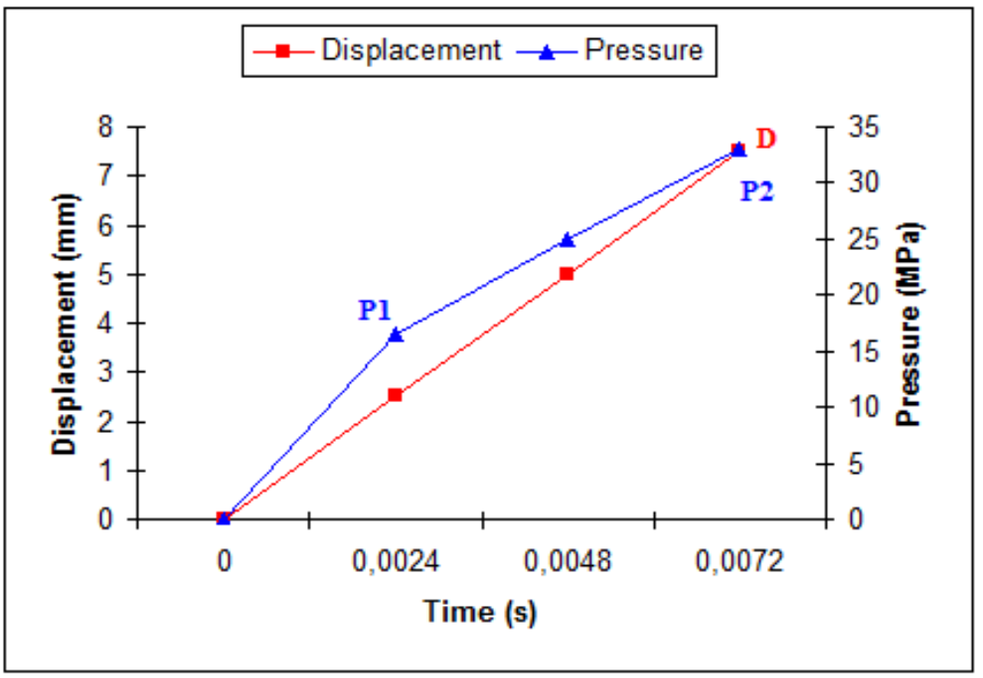

Figure 18. Definition of the design variables

5.2. Definition of the random variables

In real metal forming processes the material properties of the blank may vary within a specific range and thus probably also impact the forming results. In this work, the material of the tube is assumed to be isotropic elastic-plastic steel obeying the power-law:

$$\sigma = K\left(\varepsilon + \varepsilon_0\right)^n \tag{16}$$

where K is the strength coefficient value, n the work hardening exponent, ε_0 the strain parameter, and ε the true strain. Hardening variables (K, n) are assumed to be normal distributed with mean values μ and standard deviations σ. Friction problem plays also a key role in hydroforming process and present some scatter, to take account for this variation a normal distribution of the static friction coefficient is assumed. Finally, the initial thickness of the tube is considered as a random variable. Table 5 illustrates the statistical properties of all random parameters.

Variable	Mean value	Cov(%)	Distribution type
K(MPa)	530	5	Normal
n	0.22	5	Normal
h(mm)	1	5	Normal
μ	0.1	5	Normal

Table 5. Statistical properties of random parameters

We make the assumption that all the input parameters are considered to be statistically independent.

5.3. Evaluation of the probability of failure

Consider a total number of m stochastic variables denoted by a vector $X=\{x_1,x_2,\ldots,x_m\}^T$, in probabilistic reliability theory, the failure probability of the process is expressed as the multi-variant integral:

$$P_f = P\left(G_j(x)<0\right) = \int_{\Omega_j} f_X(x)dx_1\ldots dx_n \quad \text{where } \Omega_j : \left\{x\in\Re^n : G_j(x)<0\right\} \tag{17}$$

where P_f is the process failure probability, $f_x(X)$ is the joint probability density function of the random variables X. A reliability analysis method was generally employed since been very difficult to directly evaluate the integration in Equation (20). In the case when the problem presents a high non linearity, the use of the classical method to assess the probability of failure becomes impracticable.

Evaluation of the probability of failure is metal forming processes remain still a complicated and computational cost due to the lot of parameters that can be certain and the absence of an explicit limit state function. The appliance of the direct Monte Carlo seems impractical.

Therefore various numerical techniques have been proposed for reducing the computational cost in the evaluation of the probability of failure (Donglai et al., 2008; Jansson et al., 2007). Monte Carlo simulations coupled with response surface methodology (RSM) is used to assess the probability of failure. To build the objective function and the limit state functions given by Equations (16), (17) and (18), RSM is used based on the use Latin Hypercube design (LHD). The LHD was introduced in the present work for its efficiency, with this technique; the design space for each factor is uniformly divided. These levels are the randomly combined to specify n points defining the design matrix. Totally 50 deterministic finite element simulations were run, from these results we find a suitable approximation for the true functional relationship between response of interest y and a set of controllable variables that represent the design and random variables. Usually when the response function is not known or non Linear, a second order is utilized in the form:

$$y = \beta_0 + \sum_{i=1}^{n}\beta_i x_i + \sum_{i=1}^{n}\beta_{ii}^2 x_i^2 + \sum_{i<j}\sum_{j=1}^{n}\beta_{ij}x_i x_j + \varepsilon \tag{18}$$

where ε represents the noise or error observed in the response, y such that the expected response is $y-\varepsilon$ and β's the regression coefficients to be estimated. The least square technique is being used to fit a model equation containing the input variables by minimizing the residual error measured by the sum of square deviations. To assess the probability of failure, the limit state functions are then estimated for a new more consequent sample (1 million) starting from the model given by the response surface methodology and the probability of failure is given then by $P_f = N_{fail}/N_{total}$. N_{fail} is the number of failing points and N_{total} is the total number of simulations. This methodology will be implemented in the optimization process to optimize the loading paths with taking into account of the

uncertainty associated to the parameters defined previously. The method presented here seems more suitable since optimization of the metal forming processes is time consuming and require many evaluations of the probabilistic constraints, additional it can be used in conjunction with an optimization procedure.

In order to verify the quality of the response surface, a classical measure of the correlation between the approximate models and the exact value given by finite element simulations of the limit state function is used and shows that the approximation models can predict with a high precision the real response. Before proceeding to the reliability analysis and optimization process, the main effect plot is drawn to show how each of the variables affect severe thinning and necking. It is observed that the strength coefficient, work hardening exponent and initial thickness of the tube has the most significant impact on the severe thinning and necking plastic instabilities.

5.4. Finite element model

Figure 28 shows a finite element model (FEM) that was defined to simulate the THP. It is formed of the die that represents the final desired part, a punch modelled as rigid body and meshed with 4-node, bilinear quadrilateral, rigid element called R3D4. The tube is composed of 1340 elements (4-node, reduced integration, doubly curved shell element with five integration points through the shell section, called S4R). Since the part is symmetrical, the only quarter-model was used. The numerical simulations of the process are carried out using the explicit dynamic finite element code ABAQUS\Explicit©. The dynamic explicit algorithm seems more suitable for this simulation.

5.5. Formulation of the optimization problem

In this work, we aim to optimize the loading path under the variation of some parameters, here the objective function consist to minimize the wrinkling tendency and the probabilistic constraints was defined to avoid severe thinning and necking. We can formulate the RBDO problem as follows:

$$\begin{cases} \text{Min } f(p) \\ \text{s.c to } P\left[G_{thinning}(p,X) \le 0\right] \le Pa_i \\ \qquad P\left[G_{necking}(p,X) \le 0\right] \le Pa_i \end{cases} \tag{19}$$

where $P\left[G_i(p,X) \le 0\right]$ and Pa_i are the probability of constraint violation and the allowable probability of the i^{th} constraint violation, respectively.

A probabilistic methodology was developed and applied to optimize THP with respect to probabilistic constraint. The methodology combined an optimization strategy and probabilistic analysis. A routine is prepared with MATLAB with the use of the toolbox optimization strategy based a successive quadratic programming. The probabilistic

methodology allow to take account to the variability in metal forming process particularly is known that theses uncertainty have a significant impact on the success or the failure of the process and the quality of the final part.

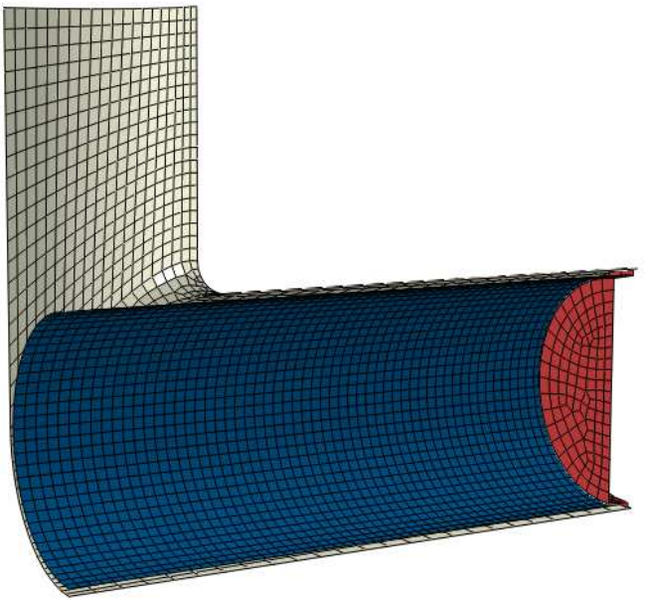

Figure 19. Finite Element Model

In general manner the RBDO is solved in two spaces physical space for the design variables and normal space when we assess the reliability index. In order to avoid calculation of the reliability and the separation of the solution in two spaces which leads to very large computational time especially for large scale structures and for high nonlinear problem like hydroforming process, the transformation approach that consist in finding in one step the probability of failure based on the predicted models and optimal design is used. In this methodology, a deterministic optimization and a reliability analysis are performed sequentially, and the procedure is repeated until desired convergence is achieved.

5.6. Results and discussion

Optimization problem is solved with different reliability level target or allowable probability of failure: $P_f = 2.28\% \Leftrightarrow \beta = 2; P_f = 0.62\% \Leftrightarrow \beta = 2.5; P_f = 0.13\% \Leftrightarrow \beta = 3$.

Table 6 resume the results obtained in the case of deterministic and reliability design for different values of the reliability index. The resolution of the problem shows that the deterministic design presents a high probability of failure for necking but an acceptable probability of failure in severe thinning, the benefits of RBDO is to ensure a level of reliability for both necking and severe thinning. The results of the optimization are reported in Table 6.

where β_1 is the reliability level for necking and β_2 for severe thinning. As shown is table 3, for the deterministic design we have a high reliability level for severe thinning compared to

the reliable design but this, it's not true for necking, in fact optimization based on reliability analysis try to find a tradeoffs between the desired reliability confidence.

Design	$D(mm)$	$P_1(MPa)$	$P_2(MPa)$	β_1	β_2
DDO	7	18	35.4643	1.6418	4.6112
RBDO $\beta = 2$	7	17.1111	35	1.9995	4.0376
RBDO $\beta = 2.5$	7	16.1165	35	2.5004	3.5679
RBDO $\beta = 3$	7.1132	14.9451	35.0035	3.0005	3.1669

Table 6. Optimal parameters for different design

The main drawback of RBDO is that it requires high number of iterations compared to deterministic approach to converge. Table 7 shows the percentage decrease of the objective function and the iterations number for the different cases.

Design	Deterministic	$\beta = 2$	$\beta = 2.5$	$\beta = 3$
% of decrease	35.7754	33.7909	30.0629	23.4896
SQP iteration	10	19	21	19

Table 7. Decrease of the objective function and number of iterations

Figure 20 presents the thickness distribution in an axial position obtained with deterministic approach and for the optimization strategy with the consideration to the probabilistic constraints. With a probabilistic approach satisfactory results are obtained to achieve a better thickness distribution in the tube (El Hami et al.,2012).

To show the effects of the introduced variability on the probabilistic constraints, a probabilistic characterization of severe thinning and necking when β=0 has been carried out. The generalized extreme value distributions type I (k=0) for severe thinning and type III (k<0)for necking seem fit very well the data. The probability density function for the generalized extreme value distribution with location parameter μ, scale parameter σ, and shape parameter $k \neq 0$ is:

$$f\left(x\middle|k,\mu,\sigma\right)=\left(\frac{1}{\sigma}\right)\exp\left(-\left(1+k\frac{\left(x-\mu\right)}{\sigma}\right)^{-\frac{1}{k}}\right)\left(1+k\frac{\left(x-\mu\right)}{\sigma}\right)^{-1-\frac{1}{k}} \tag{20}$$

For $k=0$, corresponding to the Type I case, the density is:

$$f\left(x\middle|0,\mu,\sigma\right)=\left(\frac{1}{\sigma}\right)\exp\left(-\exp\left(-\frac{\left(x-\mu\right)}{\sigma}\right)-\frac{\left(x-\mu\right)}{\sigma}\right) \tag{21}$$

The parameters that characterize these distributions are summarized in Table 8. Then we can simply assess the probability of failure of the potential failure modes to show how uncertainties can affect the probability of failure.

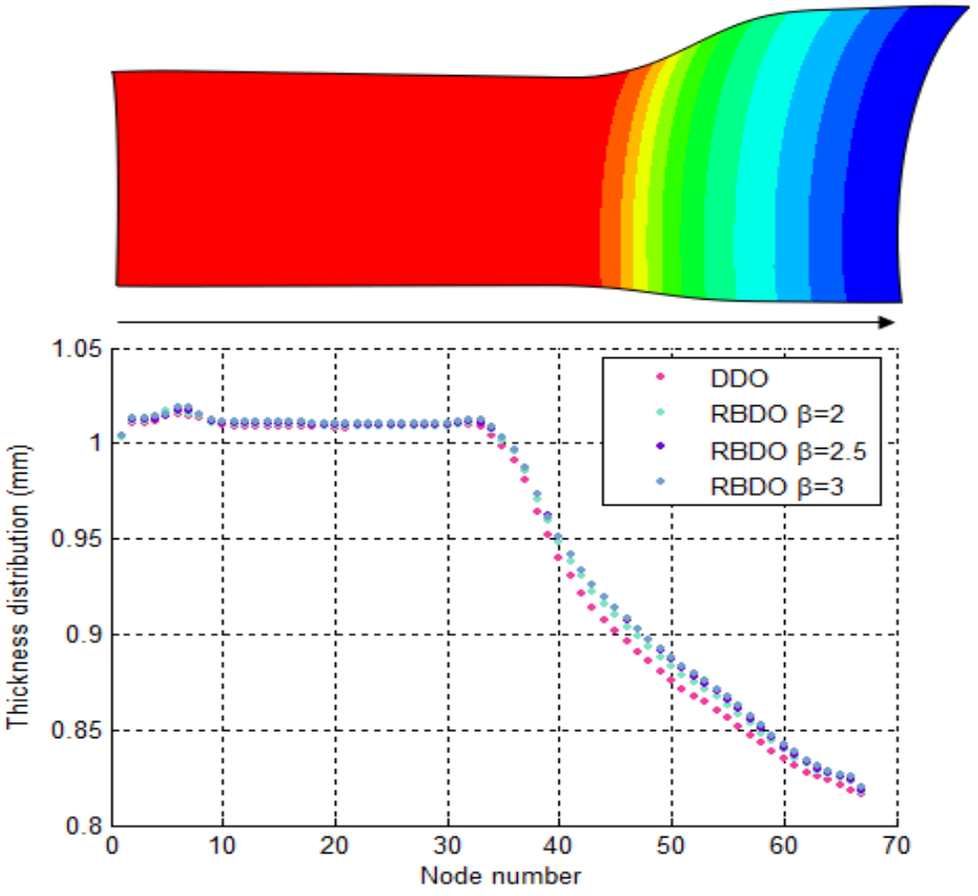

Figure 20. Thickness variation in an axial position

Parameters	μ	σ	k
$G_{necking}$	264.8466	54.1678	0
$G_{thinning}$	0.2223	0.0882	–0.0654

Table 8. Statistical parameters of the extreme value distribution

6. Conclusion

The first part of this work presents the results of a combined experimental/numerical effort that aims to assess the performance of different plastic stress flow in predicting the burst of welded steel tubes loaded under internal pressure. The prediction of the stress-strain characteristic with the anisotropic effect of tubular material has been proposed. Once the expanding diameter, the internal pressure and the wall thickness were obtained from the results of the bulge tests, the effective stress and effective strain could be calculated. The bulge tests carried out until bursting showed that all the fissures are initiated in the central area of the expanding zone not far from the weld zone.

Using the Nelder-Mead (NM) simplex search method, a flow stress curve (Swift's model) that best fits the stress-strain of the used anisotropic material could be determined with consideration global response (force/displacement). The local behaviour (stress/strain) of the welded joints and the HAZ is identified numerically using ABAQUS solver from global results (force/depth) of nanoindentation tests. The identified hardening coefficients are introduced by Swift model. From the simulations carried out, it is clear the influence of the plastic flow behaviour of the WT in the final results (thickness distribution, stress instability, tube circularity and critical thinning and rupture).

It is also clear that to predict with more accuracy the results, the model used for simulation has to be as realistic as possible. Therefore, future work in this area will include the experimental identification approach of the hardening model coupled with damage. Indeed, we think that measurements of displacements and strains without contact can improve results quality. The suggested model coupled with ductile damage can contribute to the deduction of forming limit diagrams.

The plastic deformation of a circular sheet hydraulically expanded into a complex female die was explored using experimental procedure and numerical method using ABAQUS/EXPLICIT code©. As future work, one can study others optimization techniques without using derivatives to make a numerical comparison between these different techniques and integration of adaptive remeshing procedure of sheet forming processes.

In the second part of this work, an efficient method was proposed to optimize the THP with taking into account the uncertainties that can affect the process. The optimization process consists to minimize an objective function based on the wrinkling tendency of the tube under probabilistic constraints that ensure to decrease the risk of potential failure as necking and severe thinning. This method can ensure a stable process by determining a load path that can be insensitive to the variations that can affect input parameters. Construction of the objective function and reliability analysis was done based on the response surface method (RSM). The study shows that the RSM is an effective way to reduce the number of simulations and keep a good accuracy for the optimization.

Probabilistic approach revealed several advantages and promoter way than conventional deterministic methodologies, however, probabilistic approach need precise information on the probability distributions of the uncertainty and is sometimes scarce or even absent. Moreover, some uncertainties are not random in nature and cannot be defined in a probabilistic framework.

Author details

A. El Hami
LMR, INSA de Rouen, St Etienne de Rouvray, France

B. Radi
LMMI, FST Settat, Settat, Morocco

A. Cherouat
GAMMA3, UTT, Troyes, France

7. References

Asnafi, N. & Skogsgardh, A. (2000). Theoretical and experimental analysis of stroke-controlled tube hydroforming, *Materials Science and Engineering A279*, pp. 95-110

Ayadi, A., Radi, B., Cherouat, A. & El Hami A. (2011). Optimization and identification of the characteristics of an Hydroformed Structures, *Applied Mechanics and Materials*, pp. 11-20.

Bing, L. et al. (2007). Improving the Reliability of the Tube-Hydroforming Process by the Taguchi Method, *Journal of Pressure Vessel Technology*, 129, pp. 242-247.

Cherouat, A., Saanouni, K. & Hammi, Y. (2002). Numerical improvement of thin tubes hydroforming with respect to ductile damage, *Int. J. of Mech. Sciences* 44, pp.2427-2446

Cherouat, A., Radi, B. & El Hami, A. (2008). The frictional contact of the composite fabric's shaping, *Acta Mechanica*, DOI 10.1007/s00707-007-0566-1.

Donald, B. J. & Hashmi, M.S.J. (2000). Finite element simulation of bulge forming of a cross-joint from a tubular blank, *J. of Materials Processing Technology* 103, pp. 333-342.

Donglai, W. et al. (2008). Optimization and tolerance prediction of sheet metal forming process using response surface model, *Computational Materials Science*, 42, pp. 228-233.

El Hami, A. & Radi, B. (2011). Comparison Study of Different Reliability-Based Design Optimization Approaches, *Advanced Materials Research*, pp. 119-130.

Enevoldsen, I. & Sorensen, JD. (1994). Reliability-based optimization in structural engineering, *Struct Safety*, 15, pp. 169–96.

Hama, T., Ohkubo, T., Kurisu, K., Fujimoto, H. and Takuda, H. (2006). Formability of tube hydroforming under various loading paths, *J. of Materials Processing Technology*, 177, pp. 676-679.

Jansson, T. et al. (2007). Reliability analysis of a sheet metal forming process using Monte-Carlo analysis and metamodels, *Journal of Materials Processing Technology*, 202, pp. 255-268.

Kleiber, M. et al. (2004). Response surface method for probabilistic assessment of metal forming failures, *International Journal for Numerical Methods in Engineering*, 60, pp. 51-67.

Koç, M. et al. (2002). Prediction of forming limits and parameter in the tube hydroforming process, *International Journal of Machine Tools and Manufacture*, 42, pp. 123-138.

Radi, B., Cherouat, A., Ayadi, M. & El Hami, A. (2010). Materials characterization of an hydroformed structure, *International Journal Simulation of Multidisciplinary Design Optimization*, 4, pp. 39-47.

Radi, B., El Hami, A. & Cherouat, A. (2012). Reliability Based Design Optimization Analysis of Tube Hydroforming Process, *International Journal Simulation*, in press.

Radi, B. & El Hami, A. (2007). Reliability analysis of the metal forming process, *Mathematical and Computer Modelling*, 45, pp. 431-439.

Sokolowski, T., Gerke, K., Ahmetoglu, M. & Atlan, T. (2000). Evaluation of tube formability and material characteristics: hydraulic bulge testing of tubes, *Journal of Materials Processing Technology* 98, pp. 34-40.

Youn, Byeng D, et al. (2003). A new response surface methodology for reliability-based design optimization, *Computers and structures*, 82, pp. 241-256.